LAWRENCE
LIVERMORE
NATIONAL
LABORATORY

LLNL-JRNL-752015

Radiation asymmetries during disruptions on DIII-D caused by massive gas injection

N. Commaux, L. A. Baylor, T. C. Jernigan, E. M. Hollmann, D. A. Humphreys, C. J. Lasnier

May 30, 2018

Physics of Plasmas

Disclaimer

This document was prepared as an account of work sponsored by an agency of the United States government. Neither the United States government nor Lawrence Livermore National Security, LLC, nor any of their employees makes any warranty, expressed or implied, or assumes any legal liability or responsibility for the accuracy, completeness, or usefulness of any information, apparatus, product, or process disclosed, or represents that its use would not infringe privately owned rights. Reference herein to any specific commercial product, process, or service by trade name, trademark, manufacturer, or otherwise does not necessarily constitute or imply its endorsement, recommendation, or favoring by the United States government or Lawrence Livermore National Security, LLC. The views and opinions of authors expressed herein do not necessarily state or reflect those of the United States government or Lawrence Livermore National Security, LLC, and shall not be used for advertising or product endorsement purposes.

LLNL-JRNL-752015

GA–A27717

RADIATION ASYMMETRIES DURING DISRUPTIONS ON DIII-D CAUSED BY MASSIVE GAS INJECTION

by

N. COMMAUX, L.A. BAYLOR, T.C. JERNIGAN, E.M. HOLLMANN, D.A. HUMPHREYS, J.C. WESLEY, V.A. IZZO, N.W. EIDIETIS, C.J. LASNIER, R.A. MOYER, P.B. PARKS, C. FOUST, S. COMBS, AND S. MEITNER

AUGUST 2015

GENERAL ATOMICS

DISCLAIMER

This report was prepared as an account of work sponsored by an agency of the United States Government. Neither the United States Government nor any agency thereof, nor any of their employees, makes any warranty, express or implied, or assumes any legal liability or responsibility for the accuracy, completeness, or usefulness of any information, apparatus, product, or process disclosed, or represents that its use would not infringe privately owned rights. Reference herein to any specific commercial product, process, or service by trade name, trademark, manufacturer, or otherwise, does not necessarily constitute or imply its endorsement, recommendation, or favoring by the United States Government or any agency thereof. The views and opinions of authors expressed herein do not necessarily state or reflect those of the United States Government or any agency thereof.

GA–A27717

RADIATION ASYMMETRIES DURING DISRUPTIONS ON DIII-D CAUSED BY MASSIVE GAS INJECTION

by
N. COMMAUX[1], L.A. BAYLOR[1], T.C. JERNIGAN[1], E.M. HOLLMANN[2], D.A. HUMPHREYS[3], J.C. WESLEY[3], V.A. IZZO[2], N.W. EIDIETIS[3], C.J. LASNIER[4], R.A. MOYER[2], P.B. PARKS[3], C. FOUST[1], S. COMBS[1], AND S. MEITNER[1]

This is a preprint of a paper to be submitted for publication in *Phys. Plasmas.*

[1]Oak Ridge National Laboratory, Oak Ridge, Tennessee, USA
[1]University of California-San Diego, La Jolla, California, USA
[3]General Atomics, San Diego, California, USA
[4]Lawrence Livermore National Laboratory, Livermore, California, USA

Work supported in part by
the U.S. Department of Energy
under DE-AC05-00OR22725, DE-FG02-07ER54917, DE-FC02-04ER54698,
and DE-AC52-07NA27344

GENERAL ATOMICS PROJECT 30200
AUGUST 2015

GENERAL ATOMICS

Radiation Asymmetries during Disruptions on DIII-D Caused by Massive Gas Injection

N. Commaux[1], L.R. Baylor[1], T.C. Jernigan[1], E.M. Hollmann[2], D.A Humphreys[3], J.C. Wesley[3], V.A. Izzo[2], N.W. Eidietis[3], C.J. Lasnier[4], R.A. Moyer[2], P.B. Parks[3], C.R. Foust[1], S. Combs[1], and S.J. Meitner[1]

[1]*Oak Ridge National Laboratory, Oak Ridge, TN, USA*
[2]*University of California San Diego, San Diego, CA, USA*
[3]*General Atomics, San Diego, CA, USA*
[4]*Lawrence Livermore National Laboratory, Livermore, CA, USA*

Abstract: One of the major challenges that the ITER tokamak will have to face during its operations are disruptions. During the last few years, it has been proven that the global consequences of a disruption can be mitigated by the injection of large quantities of impurities. But one aspect that has been difficult to study was the possibility of local effects inside the torus during such injection that could damage a portion of the device despite the global heat losses and generated currents remaining below design parameter. 3D MHD simulations show that there is a potential for large toroidal asymmetries of the radiated power during impurity injection due to the interaction between the particle injection plume and a large n=1 mode. Another aspect of 3D effects is the potential occurrence of Vertical Displacement Events (VDE), which could induce large poloidal heat load asymmetries. This potential deleterious effect of 3D phenomena has been studied on the DIII-D tokamak thanks to the implementation of a multi-location massive gas injection (MGI) system as well as new diagnostic capabilities. This study showed the existence of a correlation between the location of the n=1 mode and the local heat load on the plasma facing components but shows also that this effect is much smaller than anticipated (peaking factor of ~1.1 vs 3-4 according to the simulations). There seems to be no observable heat load on the first wall of DIII-D at the location of the impurity injection port as well as no significant radiation asymmetries whether one or 2 valves are fired. This study enabled the first attempt of mitigation of a VDE using impurity injection at different poloidal locations. The results showed a more favorable heat deposition when the VDE is mitigated early (right at the onset) by impurity injection. No significant improvement of the heat load mitigation efficiency has been observed for late particle injection whether the injection is done "in the way" of the VDE (upward VDE mitigated by injection from the upper part of the vessel vs the lower part) or not.

1. INTRODUCTION

Disruptions are a major concern for reliable operations of the ITER tokamak. The large radiated and conducted heat loads plus the high mechanical stress on the device due to eddy and halo currents could induce serious damage [1]. Over the past ten years, disruption mitigation experiments have shown that the preemptive injection of large quantities of impurities can mitigate the deleterious effects of disruptions significantly [2] Simple 0D metrics like radiated power fraction or halo current fraction can be increased to acceptable levels for the ITER device. But even with those criteria met, there is still the possibility that local, non-symmetric effects could reach critical limits and damage components in specific locations of the vacuum vessel. One of main concerns is the radiated power during the disruption. If 100% of the plasma thermal energy is radiated without any significant conduction, there will be no significant wall damage assuming that the radiation is homogeneous. Unfortunately, it may be possible that non-axisymmetric effects like MHD

activity or localized impurity injections could generate inhomogeneities in the radiation pattern. If the radiation toroidal peaking factor (peak value normalized to the average radiated power) in ITER is higher than 2 during a disruption, local radiated power will push the surface temperature of some Be first wall tiles beyond their melting point. Thus, understanding how to optimize radiation asymmetries during mitigated disruptions is critical in order to ensure minimal damage to the ITER device during the disruption mitigation process.

A possible source of radiation asymmetry is the MGI impurity plume itself. The local injection of large quantities (several 10s of $Pa.m^3$ in DIII-D) of highly radiative impurities such as neon may produce a large local radiated power in the vicinity of the injection port. Transport simulations combined with spectroscopic modeling and ray tracing analysis [3] predicted that such effect could induce a localized heating of the wall on ITER and DIII-D of ~100 °C above the average temperature during a rapid shutdown.

Another effect that could generate radiation asymmetries is the occurrence of large MHD instabilities during the MGI shutdown process. Recent simulations [4] using the 3D MHD code NIMROD [5] showed that MHD activity during rapid shutdown induced by an impurity injection can play a major role in the occurrence of radiation asymmetries. These simulations predict that the largest radiated power will be associated with the location where the large n=1 MHD instability mode commonly observed during disruptions stops rotating because the core heat loss due to this mode occurs at this location. This occurs systematically 180° toroidally from the impurity injection location. These predict also that due to this heat load increase opposite to the injection port, adding a second simultaneous injection to try and "spread" the heat load toroidally may worsen the peaking factor because the heat load at the location of the n=1 mode may interact with the impurities injected by the second MGI and increase locally the radiated power thus the heat load.

A final kind of inherently non symmetric disruption effect is the vertical displacement event (VDE) [6]. This kind of disruption occurs in elongated plasmas when the vertical position control of the plasma is lost (due to a hardware failure or a large transient in the plasma such has a major ELM, an H/L transition or a disruption) and the plasma hits the top or the bottom of the vessel. This kind of disruption can potentially induce large non-poloidally symmetric heat loads that could prove to be a challenge for ITER.

In this paper, results from the study of radiation asymmetries carried out on DIII-D are presented. The next section describes the experimental setup that was used in order to study asymmetries. The third section focuses on the effect that the impurity plume from MGI can have on radiated power. The potential effect of large MHD modes on the radiated power asymmetries is studied in the fourth section. Section V deals with potential radiation asymmetries generated during VDEs. To conclude, the results described in this paper as well as their potential consequences on ITER are discussed.

2. EXPERIMENTAL SETUP

These studies were achieved using two massive gas puff systems. These were located 120° apart toroidally and poloidally at 135° (MGI135D) and at 15° (MGI15U) (See Fig. 1). MGI15U consists of an array of six fast solenoid valves [7] The MGI135D system consists of an array of three fast solenoid valves [8]. These arrays were used to inject 15-50 $Pa.m^3$ of neon in ~2ms pulses into the DIII-D plasma. Neon was chosen because it is the prime candidate as the radiative impurity to be injected by the disruption mitigation system of ITER

[9]. The target plasma for the DIII-D radiation asymmetry experiments was an ITER-like lower single null H mode plasma. The scenario parameters were a toroidal field of 2.05T, plasma current of 1.5MA, neutral beam power of 2MW and ECH power of 3.2MW. This resulted in a plasma discharge with an edge safety factor q_{95} of 3.9, central electron temperature and density of 2.5 keV and 6.5×10^{19} m^{-3} repectively, a pedestal electron temperature and density of 700 eV and $6e10^{19} m^{-3}$ repectively, a thermal and magnetic energy content of 820 kJ and 750 kJ res.pectively.

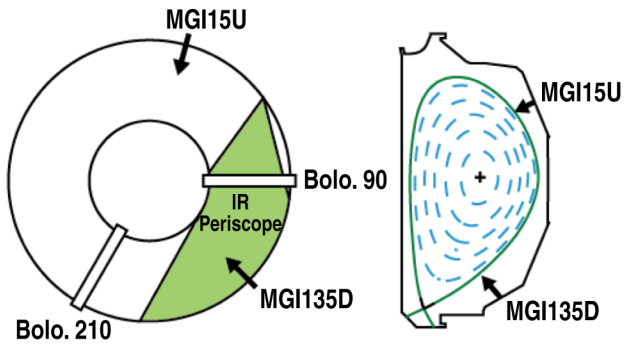

Fig. 1. DIII-D disruption massive gas puff systems (MGI15U and MGI135D) and diagnostics layout.

The radiated power during a neon shutdown is dominated by neon line emission without the sputtered lower Z wall material playing a significant role in the radiative heat dissipation unlike natural disruptions. This fact has already been observed on metal wall devices such as JET that switched recently from carbon plasma facing components to ITER-like metal plasma facing components [10]. This helps extrapolate the results of these experiments on DIII-D (carbon wall) to ITER (metal wall). This change affected the radiated power and time scales during natural disruptions but had no significant effect on the characteristics of high Z MGI mitigated disruptions [10].

The main diagnostics that were used for these experiments were 2 fast bolometer poloidal arrays (at 90° and 210°) used to determine the radiated power at different poloidal and toroidal locations and a new infrared periscope [11] The locations of these diagnostics with respect to MGI15U and MGI135D are shown on Fig. 1. This setup enables for the first time a full infrared coverage of an MGI port (MGI135D) which was useful to study potential local heat loads at the injection port compared to other plasma facing components (PFC) surfaces further from the injection location.

3. INFLUENCE OF THE MGI IMPURITY PLUME ON RADIATION ASYMMETRIES

One of the major concerns with MGI is the possibility of localized radiation related to the location of the gas injection. For example there is a possibility of a potential localized heat load generated in the vicinity of the injection port by the highly radiative impurity plume created by the MGI system during the injection [12]. Simulations predict that this localized heat load could account to a local elevation of the temperature of the first wall of ~100 °C above the background [3] which in some cases on ITER could “push” the temperature of the tiles surrounding the injection port above their melting point. If such localized heat loads exist, there is a possibility that using more than one injection location may “smear” the heat loads and generate a more homogeneous power deposition around the torus. In order to assess the existence of localized heat loads related to the injection location and how to mitigate them, an experiment using both MGI arrays (MGI15U and MGI135D) was executed on DIII-D. This experiment consisted of firing MGI15U and MGI135D alone on the plasma target described in Section II and then fire them both with a set delay between the 2 injections and varying that delay from shot to shot. The goal of this experiment was to determine how the radiated power pattern (measured by fast bolometers) evolved between single injection and

dual injection and also as a function of the delay in the dual injection cases during all three phases of the shutdown. These are the pre-thermal quench (pre-TQ) which is the phase between the first MGI firing time and the onset of the thermal quench, the thermal quench (TQ) which is the phase during which the plasma loses its thermal energy and the current quench (CQ) which is the phase during which the plasma current decays to 0. Figure 2 shows the radiated power asymmetry factor between the 2 bolometer arrays at 90° and 210° as a function of the delay between the MGI15U and MGI135D firing times during all 3 phases of the fast shutdown. The cases for which only one valve fired are indicated by +/- ∞. This asymmetry factor is the ratio between the difference of radiated energy measured by the 2 arrays and the total radiated energy measured by the 2 arrays: $\frac{W_{90} - W_{210}}{W_{90} + W_{210}}$ where W_{90} is the radiated energy measured at 90° and W_{210} is the radiated energy measured at 210°. This figure shows clearly that a significant asymmetry occurs during the pre-TQ but largely disappears during the TQ and CQ. The pre-TQ radiated energy accounts only for 10-20% of the total radiated power during the shutdown process. Most of the energy is radiated away during the TQ and CQ, which appear according to the bolometer data to be very symmetric. The data shows no significant correlation between the asymmetry factor and the location of the injection in the single injection cases and the delay between MGI15U and MGI135D when both systems were fired in the same shot. In the hypothesis of a significant heat load in the vicinity of the MGI system firing first, one could expect to measure more radiated energy on the 90° bolometer array when MGI15U is firing first (since it is only 75° toroidally away from that array versus 165° for the 210° array). With MGI135D firing first one would expect a more symmetric measurement between the 2 bolometers since it is 45° away from the 90° array and 75° away from the 210° array. Instead, no significant variation is observed regardless of when MGI15U or MGI135D is firing. Of course this localized radiation could be highly peaked around the injection port. This could make it difficult to detect by the bolometer system of DIII-D due to its limited Toroidal coverage.

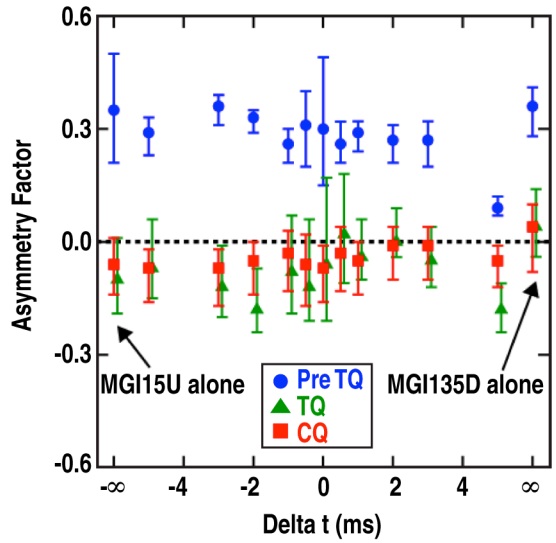

Fig. 2. Asymmetry factor $\frac{W_{90} - W_{210}}{W_{90} + W_{210}}$ as a function of the delay between MGI15U firing time and MGI135D firing time during 3 phases of the disruption: circles for pre-TQ, triangles for TQ and squares for CQ.

But the most important fact showing this is the direct \measurements of the wall temperature using the IR periscope. The peak wall temperature resulting from the rapid shutdown was determined using data from the IR periscope to calculate the surface temperature of the PFC tiles through a black body model. The IR periscope having too slow a frame rate to capture the details of the shutdown, the peak temperatures during shutdown were determined by extrapolating backward the PFC temperatures while the wall was cooling down after the end of the shot over a period of 40ms (temperature decay is quasi-linear during such a short period of time). An example of such an extrapolation is provided in Fig. 3. The resulting temperature data is shown in Fig. 4 as well as the location of different regions of interests used to compare wall temperatures in this paper. Of course what really matters to assess the heat flux during a disruption is the temperature elevation during the disruption but the temperature of the main chamber (divertor excluded) during those experiments is too low to be measured using the IR periscope when in disruption setup. Thermocouple data show that it was ~30 °C (divertor excluded). Thus the peak temperature measured during these

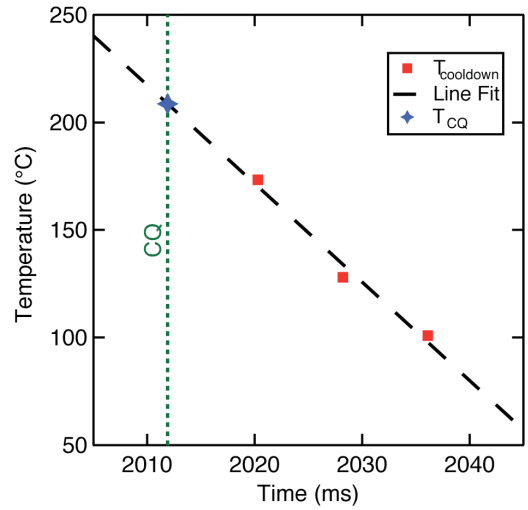

Fig. 3. Example of extrapolation of the temperatures in Region1 (see Fig. 4) during the cooldown following a disruption ($T_{cooldown}$) providing the temperature of the wall at the moment of the CQ (T_{CQ}) through a simple linear fit.

experiments was a good measurement of the temperature elevation. The specific issue of potential localized heat loads in the vicinity of the injection location could be addressed thanks to the IR coverage of the MGI135D port. The wall temperatures were averaged in the region surrounding MGI135D and in region 1 (see Fig. 4). Region 1 was selected as representative of the general behavior of the first wall away from the MGI port. Any significant heat load in the vicinity of MGI135D when it is firing could be detected by a resulting higher temperature compared to region 1, which is further from MGI135D. The

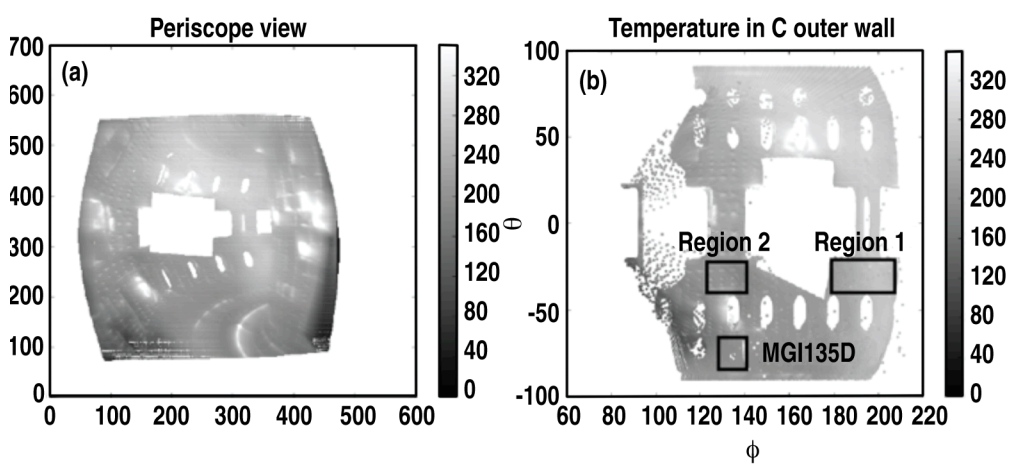

Fig. 4. Extrapolated peak temperatures (in ºC) for the field of view of the IR periscope (a) and the resulting mapping of the outer wall (b). The location of different regions of interests and of the MGI 2 are shown.

result of this comparison is shown in Fig. 5. This shows clearly that the region surrounding MGI135D is always cooler by almost 100°C compared to region 1. This difference could be due to differences in the characteristics of the tiles surrounding the MGI135D port. There is an observable trend showing that the region surrounding MGI135D gets hotter when MGI135D is firing first or alone but that same trend is also followed in region 1. The fact that the vacuum vessel as a whole seems hotter when MGI135D is firing first could be explained by intrinsic differences of the injection characteristics of the MGI135D valve array compared to MGI15U. It appears that a slightly stronger gas flow is generated by MGI135D which apparently induces a slightly higher radiative fraction during the fast shutdown thus, a higher heat flux to the main chamber compared to MGI15U. But this global difference shows that no localized heat load in the vicinity of the injection port can be observed. This contradicts the simulations that predict a local temperature increase of ~100 °C solely due to the impurity plume distribution since no MHD effect was taken into account in simulations of the radiating plume. The fact that this effect appears much weaker is probably due to the fact that the radiation process is dominated by other effects than the simple distribution of impurities in the plasma. A similar experiment was carried out in 2012 on Alcator C-mod [13] with a different MGI configuration: The two MGI valves on C-mod were localized ~180º apart toroidally both at the outer midplane. There was a discrepancy with the DIII-D results for the case of simultaneous injection. On C-mod relatively large toroidal peaking factors (up to 2) were measured when both valves were fired simultaneously, whereas, their results were similar for single valve injection or with large delays between injections (peaking factor close to 1). This difference might be due to the difference in implementation of the valve systems around the torus (n/m=2=1/2 for C-mod vs 1/1 for DIII-D) that may in the case of C-mod enhance the interaction between the injected impurities and inherent MHD activity in the plasma. If the mode structure interacts with the impurity plume, it could increase locally the radiated power, which could increase the risk of localized damage to the wall.

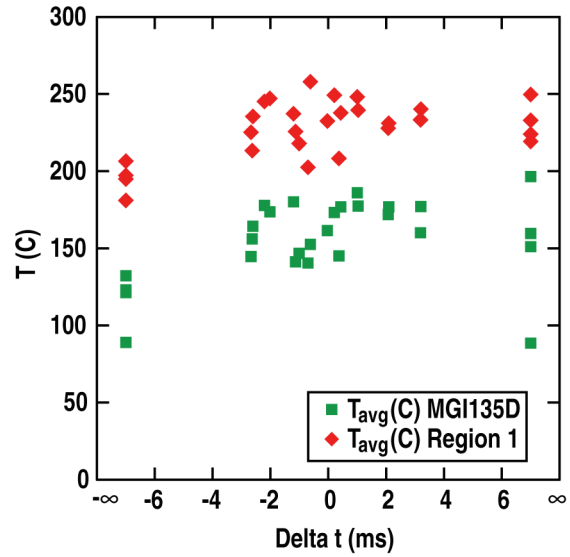

Fig. 5. Average wall temperatures around the MGI135D (squares) port and in Region 1 (diamonds) (see Fig. 4) as a function of the delay between MGI15U firing time and MGI135D firing time.

4. INFLUENCE OF MHD ACTIVITY DURING THE MGI SHUTDOWN ON RADIATION ASYMMETRIES

The occurrence of large low-n MHD modes during an MGI shutdown has been commonly observed on multiple devices [14,15]. These modes can generate large localized particle and energy exchanges between the core and the edge. A concern is that these may induce large radiation asymmetries by interacting with the MGI impurities. In order to evaluate if this effect could be significant, 3D MHD simulations of DIII-D plasmas subjected to an MGI were carried out using the NIMROD MHD code [4]. The MGI was simulated by an instantaneous toroidally and poloidally localized deposition of impurities. The results of these simulations

showed that strong toroidal radiation asymmetries can be induced by a large n=1 MHD mode due to the large non-axisymmetric radial particle flows that expel a large amount of particles to the edge. Depending on the impurity transport coefficients, these simulations predicted a toroidal radiated power peaking factor (peak power normalized to average) that can vary from 1 up to 4.

In order to test this predicted effect of MHD on radiated power asymmetries, an experiment was carried out on DIII-D. It consisted of using the non-axisymmetric in-vessel coils of DIII-D (I coils) to generate an artificial n=1 error field in order to force the toroidal phase of the n=1 MHD mode by forcing it to stop rotating at a certain location (normally these modes tend to always lock on DIII-D at the same location: ~260º probably due to intrinsic error fields). The toroidal phase of this artificial error field was then varied by 90° steps from shot to shot in order to scan the toroidal phase of the n=1 mode generated during the MGI shutdown.

Only one valve (MGI15U) was used in this experiment. By using the fast bolometer arrays and the IR periscope, it was then possible to evaluate the effect of the toroidal phase of the mode on the radiated power pattern during the shutdown. This method to scan the phase of the n=1 mode proved efficient as shown in Fig. 6. This figure shows that the mode's phase is clearly influenced by the phase of the applied error field though with a ~60º offset that may be related to the plasma rotation. The radiated power asymmetry factor is shown in Fig. 7. This figure shows a significant variation of the radiated energy measured by the 90º and 210º arrays during the TQ with the phase of the applied error field. This could indicate a toroidal radiating pattern that changes location with the applied error field, which is consistent with the hypothesis of an influence of the MHD activity on the radiated power. However, due to the limited toroidal coverage of the bolometer system, these measurements could underestimate the real toroidal peaking factor. The consequences of this effect on the wall temperature were also studied. The average wall temperature in region 1 and 2 (see Fig. 4) are shown in Fig. 8. This figure shows that the average wall temperature may vary slightly when the toroidal phase of the n=1 field is changed. The phase of this variation with respect to the error field toroidal

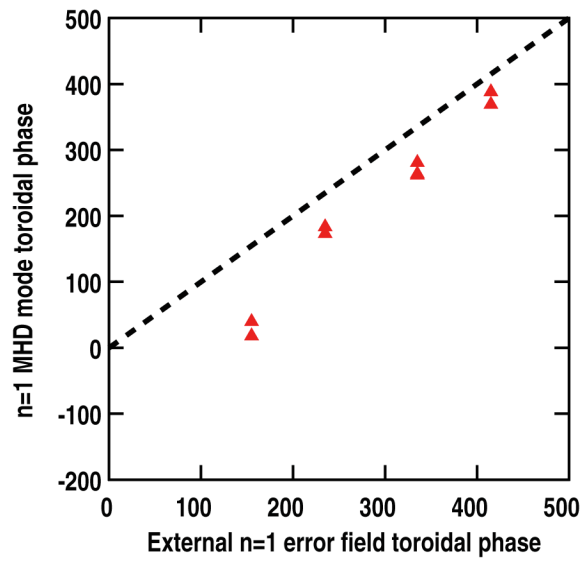

Fig. 6. Toroidal phase of the n=1 MHD mode triggered during the MGI shutdown as a function of the toroidal phase of the applied n=1 error field using the I.

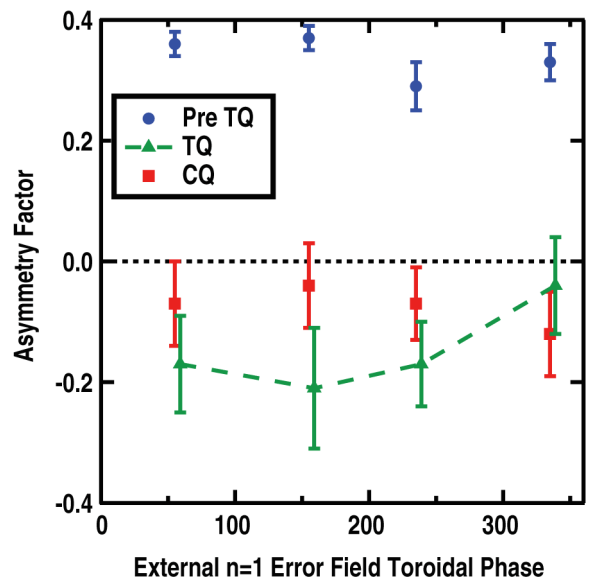

Fig. 7. Evolution of the radiated power asymmetry factor (see Fig. 2) as a function of the toroidal phase of the applied n=1 error field during 3 phases of the disruption: circles for pre-TQ, triangles for TQ and squares for CQ.

phase is not the same for the two regions, suggesting a toroidally and/or poloidally localized MHD effect although the exact toroidal and poloidal structure of this radiative pattern is difficult to resolve on DIII-D due to a limited diagnostic coverage.

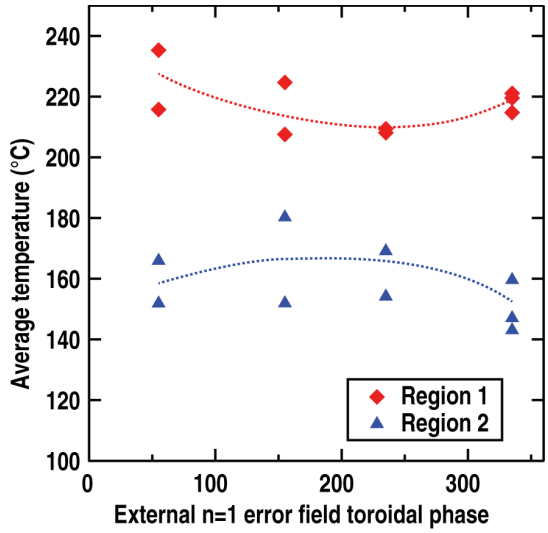

Fig. 8. Evolution of the average wall temperature measured by the IR periscope in Region 1 (diamond) and 2 (triangle) (see Fig. 3) as a function of the toroidal phase of the applied n=1 field.

These results confirm that radiated power asymmetries are influenced by the large n=1 mode generated during an MGI shutdown as predicted by the NIMROD simulations since the toroidal phase where the mode locks as an effect on the local radiated energy and resulting wall temperature. But these asymmetries seem much smaller than predicted by the simulations which were anywhere from 2 to 4 although again the limited toroidal coverage makes this assessment difficult.

5. ASYMMETRIES INDUCED BY VERTICAL DISPLACEMENT EVENTS

VDE are a major concern for large tokamak such as ITER. These events consist of a loss of vertical position control of the plasma resulting in the plasma moving rapidly to the top or bottom of the vessel. The vertical position control can be lost due to large plasma transients (H/L transition, large ELM etc.) that can suddenly change the normalized inductance of the plasma or a hardware failure (position control coil power supply failing etc.) [16]. These events can induce very large poloidally asymmetric heat loads (poloidal peaking factor in excess of 2 observed on DIII-D). Most of the heat is typically conducted to the wall at the location where the plasma touches the plasma facing components. Thus understanding how these heat loads can be mitigated is critical to the reliable operation of ITER.

In order to test VDE mitigation on DIII-D, a method to reliably trigger VDE was designed. It consists of simultaneously kicking the plasma upward or downward using the poloidal coils while shutting down the vertical control. By picking which coil to ramp up, the direction of the VDE can be controlled (lower coil for an upward VDE and upper coil for a downward VDE). This method enabled reliable VDE triggering with excellent reproducibility (all VDE timings are within 1-2 ms). Using this VDE triggering scenario, one of the MGIs was fired in order to mitigate the heat loads. The DIII-D configuration enabled for the first time to test the effect of the position of the MGI valve with respect to the direction of the VDE (upward or downward) since the two MGI systems are at different poloidal locations: MGI15U is firing from the upper part of the vacuum vessel and MGI135D from the lower part

of the vessel (see Fig. 1). The hypothesis would be that an MGI valve located in the "way" of the VDE (for example a valve in the upper part of the vessel for an upward VDE) would introduce impurities faster into the plasma, thus mitigating heat loads more efficiently by radiating away the plasma energy before it hits the wall.

For this experiment the delay time was varied between the MGI firing time and the moment the plasma hits the wall (characterized by the CQ onset time for the unmitigated case). Also, the direction of the VDE and the location of the firing MGI valve were scanned from shot to shot. The results for downward VDE mitigation using either MGI135D or MGI15U are shown in Fig. 9. This figure shows the variation of the radiated energy and the lower divertor peak heat flux as a function of the delay between the MGI firing time and the TQ onset time for the unmitigated case. This delay was varied from 15ms before the TQ (onset of the VDE movement) to 0ms with the TQ (simultaneous with the plasma hitting the wall). These figures show that the delay time between the MGI firing time and the moment the plasma touches the wall is critical for an efficient mitigation of the heat loads. Figure 9a shows that the radiated power measured by the fast bolometer arrays increases by a factor of ~3 for an early mitigation (15ms before the plasma would hit the wall without mitigation) compared to the unmitigated case (1.1MJ vs 0.4MJ). A larger radiated power is very favorable to protect the wall because the radiated power will be deposited homogeneously while conducted heat load would be deposited on a much smaller area. This measurement is confirmed by the peak heat flux measured using the fast IR camera. Figure 9b shows that this peak heat load on the lower divertor drops by a factor of 3 compared to the unmitigated case. When the MGI firing time is much later, the mitigation becomes much less efficient. For example in the case the MGI is fired exactly at the time the plasma hits the wall (t_{MGI}-t_{CQ} = 0 in Fig. 9), the heat load to the divertor is equivalent (within experimental uncertainties) to the one observed during an unmitigated VDE. Thus timing is critical for an efficient mitigation of VDE.

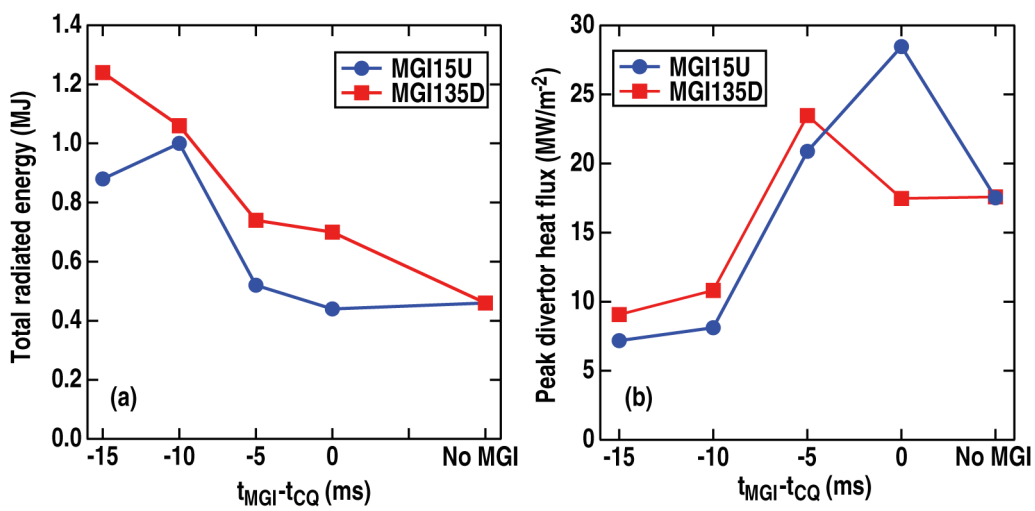

Fig. 9. Evolution of the radiated energy measured by the 90º bolometer array (a) and the peak heat flux (b) measured by the IR periscope in the lower divertor as a function of the delay between the MGI firing time and the TQ onset time for an unmitigated VDE using MGI135D (squares) and MGI15U (circles).

Concerning the test of the MGI injection geometry with respect to the direction of the VDE, unfortunately, a direct comparison between MGI135D and MGI15U was made difficult

by inherent differences in the resulting flow rates the systems can deliver. It appears that because of differences in the implementation of the 2 systems, MGI135D is capable of delivering larger flows and ram pressures than MGI15U (as observed also in section III). In order to test the influence of the injection geometry, the mitigation efficiency was compared between downward VDE vs upward VDE while always using only the upper system MGI15U for mitigation. The results of this comparison are shown in Fig. 10. This figure shows that there is a slight increase in radiated power (5-10%) for upward VDEs. This could mean that the upper MGI is slightly more efficient for the mitigation of VDEs going toward the MGI array vs VDE going away from the MGI system. But this difference is small especially considering the ~10% scatter observed in measured radiated power for similar VDE cases.

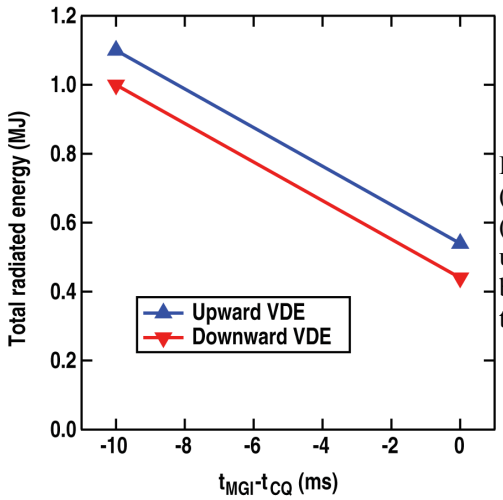

Fig. 10. Total radiated energy during upward (triangles pointing up) and downward (triangles pointing down) VDE mitigated using MGI15U as a function of the delay between the MGI firing time and the CQ of the unmitigated VDE.

These results show clearly that an efficient mitigation of VDEs heat loads is possible using impurity injection and that the timing of this injection with respect to the moment the plasma strikes the wall for an efficient mitigation. The location of the mitigation system with respect to the direction of the VDE doesn't seem to have a significant effect.

6. CONCLUSION AND PROSPECTS FOR ITER

The radiation asymmetries observed during massive gas injection on DIII-D during the thermal quench were significantly lower than expected. Radiation induced directly by the impurity plume appears quite small on DIII-D with no observable heat load detected around the injection port and no significant radiation asymmetries observed during the main phase of the shutdown: the thermal quench and the current quench. This indicates that there may be no disadvantage to injecting impurities in ITER from a single location from a heat load mitigation point of view. Experiments indicate that TQ MHD does affect TQ radiation symmetry as predicted by NIMROD 3D MHD simulations. However, the effect is smaller than expected (observed asymmetries of 10% vs factor of 2 or more according to NIMROD) although more detailed experiments will be required to determine the real peaking factor due to the limited toroidal coverage of the bolometric diagnostics on DIII-D. This could be a concern for ITER in the future since this interaction between the MHD mode and the radiating impurities if the MHD mode toroidal phase corresponds to the location of the MGI injection could increase locally the radiation (because of the energy expelled locally by the MHD mode interacting with the impurities from the MGI) and generate radiation toroidal peaking factor larger than acceptable on the ITER device. The factors influencing the toroidal phase of the

n=1 mode will have to be studied in more detail in order to prevent such interaction between the MHD mode and the MGI impurity plume.

VDEs are a major concern in terms or radiation asymmetries on ITER. These experiments on DIII-D have demonstrated that the massive injection of impurities early enough (15 ms on DIII-D) is very efficient at reducing dramatically the asymmetric conducted heat loads (heat flux reduced by a factor of 3). This timing is essential for a good mitigation. No real benefits were observed whether the injection was in the path of the VDE or not. On DIII-D the best mitigation was observed for MGI fired right at the onset of the VDE (vertical movement of a few cm). This would be rather easy to achieve on ITER, since the onset of a VDE can be easily detected by the magnetic probes and the whole timescale of a VDE on ITER is much slower than on DIII-D (hundreds of ms vs 10-20 ms). Thus, an early mitigation on ITER should be achieved.

One of the topics that remain to be explored concerning the understanding and mitigation of 3D heat loads during disruptions is the effect that a deeper impurity injection technique such as pellet injection techniques [17] (which are favored on ITER) would have since the transport of impurities and local plasma conditions where the bulk of the impurities are could change radically.

Acknowledgement

This work was supported by the U.S. Department of Energy under DE-AC05-00OR22725, DE-FG02-07ER54917, DE-FC02-04ER54698, and DE-AC52-07NA27344. DIII-D data shown in this paper can be obtained in digital format by following the links at https://fusion.gat.com/global.D3D_DMP.

References

[1] M. Sugihara, M. Shimada, H. Fujieda, Yu. Gribov, K. Ioki, Y. Kawano, R. Khayrutdinov, V. Lukash and J. Ohmori Nucl. Fusion **47** (2007) 337

[2] P. L. Taylor, A. G. Kellman, T. E. Evans, D. S. Gray, D. A. Humphreys, A. W. Hyatt, T. C. Jernigan, R. L. Lee, J. A. Leuer, S. C. Luckhardt, P. B. Parks, M. J. Schaffer, D. G. Whyte and J. Zhanga, Phys. Plamas **6** (1999) 1872

[3] E. M. Hollmann, D. A. Humphreys and P. B. Parks, Nucl. Fusion **52** (2012) 033001

[4] V. A. Izzo Phys. Plamas **20** (2013) 056107

[5] C. R. Sovinec, A. H. Glasser, T. A. Gianakon, D. C. Barnes, R. A. Nebel, S. E. Kruger, D. D. Schnack, S. J. Plimpton, A. Tarditi, and M. S. Chu and the NIMROD Team, J. Comput. Phys. **195** (2004) 355

[6] E. Hollmann, N. Commaux, N. W. Eidietis, D. A. Humphreys, T. J. Jernigan, C. J. Lasnier, R. A. Moyer, R. A. Pitts, M. Sugihara, E. J. Strait, J. Watkins and J. C. Wesley Phys. Plamas **20** (2013) 062501

[7] J. C. Wesley, E. M. Hollmann, T. C. Jernigan, M. A. Van Zeeland L. R. Baylor, J. A. Boedo, S. K. Combs, T. E. Evans, M. Groth, D. A. Humphreys, A. W. Hyatt, V. A. Izzo, A. James, R. A. Moyer, P. B. Parks, D.L. Rudakov, E. J. Strait, W. Wu, and J. H. Yu *Proc. 22nd IAEA Fusion Energy Conference* (Geneva) (2008)

[8] S. L. Milora, S. K. Combs and C.R. Foust Rev. Sci. Instruments **57** (1986) 2356

[9] S. Maruyama, Y. Yang, R.A. Pitts, M. Sugihara, S. Putvinski, S. Carpentier-Chouchana, B. Li, W. Li, L.R. Baylor, S.J. Meitner, C. Day, B. LaBombard and M. Reinke IAEA FEC Conference (2010) ITR/P1-28

[10] M. Lehnen, G. Arnoux, S. Brezinsek, J. Flanagan, S.N. Gerasimov, N. Hartmann, T. C. Hender, A. Huber, S. Jachmich, V. Kiptily, U. Kruezi, G.F. Matthews, J. Morris, V. V. Plyusnin, C. Reux, V. Riccardo, B. Sieglin, P.C. de Vries and JET EFDA Contributors Nucl. Fusion **53** (2013) 093007

[11] C. J. Lasnier, S. L. Allen, M. E. Fenstermacher, D. N. Hill and T. R. Weber *Proc. 53rd APS DPP Conference* (Salt Lake City) (2011)

[12] E. M. Hollmann, T. C. Jernigan, P. B. Parks, J. A. Boedo, T. E. Evans, M. Groth, D. A. Humphreys, A. N. James, M. J. Lanctot, D. Nishijima, D. L. Rudakov, H. A. Scott, E. J. Strait, M. A. Van Zeeland, J. C.Wesley,W. P.West, W. Wu and J. H. Yu Nucl. Fusion **48** (2008) 115007

[13] G. M. Olynyk, R. S. Granetz, M. L. Reinke, D. G. Whyte, T. Golfinopoulos, J. W. Hughes, J. R.Walk, V. A. Izzo, S.K. Combs, S. L. Milora and M. W. Brookman Nucl. Fusion **53** (2013) 092001

[14] C. Reux, J. Bucalossi, F. Saint-Laurent, C. Gil, P. Moreau and P. Maget, Nucl. Fusion **50** (2010) 095006

[15] R. S. Granetz, E. M. Hollmann, D. G. Whyte, V. A. Izzo, G. Y. Antar, A. Bader, M. Bakhtiari, T. Biewer, J. A. Boedo, T. E. Evans et al., Nucl. Fusion **47** (2007) 1086

[16] D. A. Humphreys, T. A. Casper, N. Eidietis, M. Ferrara, D. A. Gates, I. H. Hutchinson, G. L. Jackson, E. Kolemen, J. A. Leuer, J. Lister, L. L. LoDestro, W. H. Meyer, L. D. Pearlstein, A. Portone, F. Sartori, M. L. Walker, A. S.Welander and S. M. Wolfe Nucl. Fusion **49** (2009) 115003

[17] N. Commaux, L .R. Baylor, T. C. Jernigan, E. M. Hollmann, P. B. Parks, D. A. Humphreys, J. C.Wesley and J. H. Yu Nucl. Fusion **50** (2010) 112001